EDGE ARTICLE

Aggregation-induced emission enhancement of a *meso*-trifluoromethyl BODIPY *via* J-aggregation†

Sohee Choi,[a] Jean Bouffard[b] and Youngmi Kim*[a]

A CF$_3$-BODIPY forms strongly luminescent aggregates, which contrasts with the quenched condensed-phase photophysics that are typical for BODIPY dyes. Examination of the luminescent properties of these aggregates – narrow red-shifted absorption and emission bands, minimal Stokes shift and increased fluorescence rate constants – and of the solid-state packing of the dye establish the CF$_3$-BODIPY as the first structurally characterized genuine BODIPY J-aggregate.

Introduction

4,4-Difluoro-4-bora-3*a*,4*a*-diaza-*s*-indacene (difluoroboron dipyrromethene or BODIPY) dyes are among the most popular organic fluorophores and have been widely employed as labeling reagents in molecular biology,[1] lasing media in liquid solution dye lasers,[2] and chemosensors or molecular probes.[3] The widespread interest in BODIPY dyes derives from their excellent spectroscopic properties, high photochemical and chemical stabilities, and from the facile alteration of their photophysical properties by molecular design.[4] However, while many BODIPY dyes exhibit high fluorescence quantum yields in dilute solutions ($\Phi_F > 0.5$), they scarcely emit in the solid state as a result of emission quenching upon aggregation, which remains a major challenge in the application of BODIPY dyes.[5]

To preserve or even improve photophysical properties in the solid state, several strategies have been exploited, especially structural modification by appending bulky groups,[6] such as dendrons,[7] and, more recently, innovations in aggregation-induced emission enhancement (AIEE).[8] A promising approach to improve the photophysical properties of dyes in aggregated solid states is to engineer their packing to favor the formation of emissive J-type aggregates (head-to-tail), wherein the transition dipoles of the monomeric dyes align in a coplanar inclined fashion with a slip angle $\theta < 54.7°$ (Fig. 1A).[9] These aggregates, following the molecular exciton coupling model,[10] exhibit large bathochromic shifts in their absorption spectra relative to the monomers, together with very small Stokes

shifts, narrow transition bands, and increased fluorescence intensity.

To date there has not been an unambiguous report of the isolated formation, nor of the structural characterization of J-aggregates among monomeric chromophores of the BODIPY family. The formation of mixed non-fluorescent H-aggregates and fluorescent J-aggregates has recently been observed by Johansson and coworkers in BODIPY-labeled proteins and BODIPY-labeled lipid phases,[11] and in BODIPYs substituted with bulky adamantyl groups by Vu and coworkers.[12] The latter also reported that the introduction of highly sterically demanding substituents on the BODIPY can prevent emission quenching caused by intermolecular π–π stacking, and avoid the formation of tightly packed aggregates altogether.[13] Others have observed the formation of red-shifted, relatively narrow

[a]*Department of Chemistry, Institute of Nanosensor and Biotechnology, Dankook University, 126 Jukjeon-dong, Yongin-si, Gyeonggi-do, 448-701, Korea. E-mail: youngmi@dankook.ac.kr; Fax: +82 31 8005 3148; Tel: +82 31 8005 3156*

[b]*Department of Chemistry and Nano Science, and Global Top5 Research Program, Ewha Womans University, 52 Ewhayeodae-gil, Seodaemun-gu, Seoul 120-750, Korea*
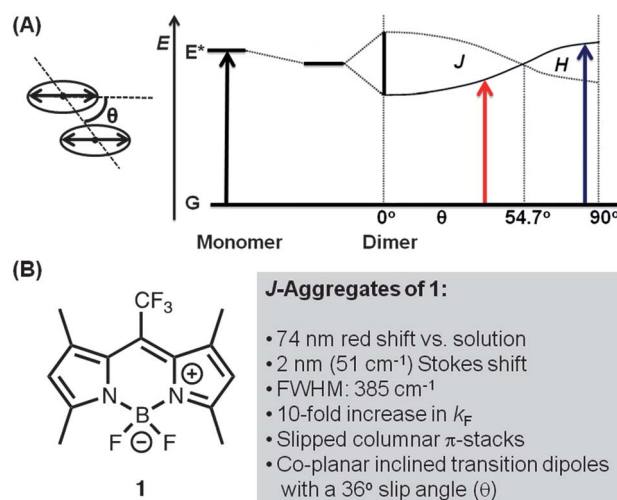
Fig. 1 (A) Exciton band energy diagram for a molecular dimer with coplanar inclined transition dipoles. Transition dipole moments are indicated as double arrows in the dimer aggregates with a slip angle θ. (B) Characteristics of the J-aggregates of CF$_3$-BODIPY **1**.

J-Aggregates of **1**:
- 74 nm red shift vs. solution
- 2 nm (51 cm^{-1}) Stokes shift
- FWHM: 385 cm^{-1}
- 10-fold increase in k_F
- Slipped columnar π-stacks
- Co-planar inclined transition dipoles with a 36° slip angle (θ)

absorption and/or emission bands consistent with J-type packing in the aggregated phase of BODIPY derivatives, but lacked experimental evidence to confirm the microstructure of these aggregates.[14]

In this edge article, we present the first unequivocal example of a structurally characterized emissive BODIPY J-aggregate, formed by the simple *meso*-trifluoromethyl-substituted dye **1** (CF$_3$-BODIPY). The dye features the signature photophysical properties associated with J-aggregates, and the classical head-to-tail solid-state organization that leads to these properties.

Results and discussion

The synthesis of *meso*-CF$_3$-substituted BODIPY **1** is straightforward, as shown in Fig. 2A. CF$_3$-BODIPY **1** was prepared in moderate yield from the condensation of 2,4-dimethylpyrrole with 2-trifluoroacetyl-3,5-dimethylpyrrole, followed by complexation with BF$_3 \cdot$Et$_2$O. CF$_3$-BODIPY **1** is very soluble in all common organic solvents, but completely insoluble in water. The reference *meso*-substituted methyl congener (CH$_3$-BODIPY **2**; Fig. 2B), was prepared from 2,4-dimethylpyrrole and acetyl chloride according to reported procedures (Scheme S2†).[15]

The spectroscopic features of **1**, which has a strongly electron-withdrawing CF$_3$ group, are distinct from those of the congener with a methyl substituent, **2**, in both the solution and solid state. In CHCl$_3$ solution, **1** displays remarkably red-shifted absorption and emission maxima ($\lambda_{\mathrm{max,abs}}$ = 553 nm, $\lambda_{\mathrm{max,em}}$ = 622 nm) by comparison with those of **2** ($\lambda_{\mathrm{max,abs}}$ = 499 nm, $\lambda_{\mathrm{max,em}}$ = 520 nm), broad absorption and fluorescence bands, and a large Stokes shift (Fig. 2C and Table S1†). The bathochromic electronic transitions observed for **1** are consistent with the calculated reduced HOMO–LUMO gap (Fig. 3),[16] which predominantly arises from a stabilization of the LUMO by the electron-withdrawing CF$_3$ substituent. The extent of the red-
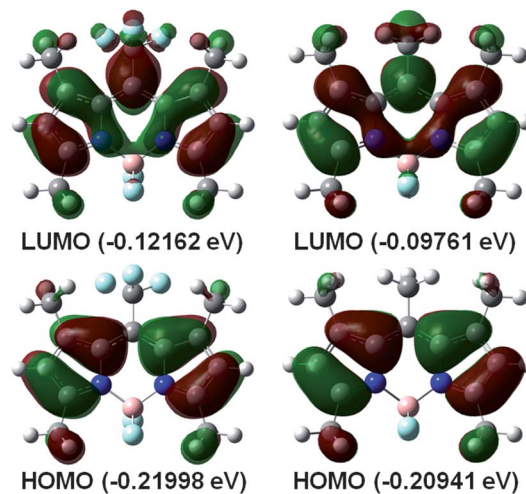
Fig. 3 Calculated frontier molecular orbitals for **1** (left) and **2** (right) and their orbital energies (eV).

shift induced by this simple modification of the BODIPY scaffold compares favorably with more synthetically intricate approaches such as the introduction of styryl groups[17] or pyrrole ring fusion.[18]

Compound **1** is poorly luminescent in chloroform solution due to its reduced molar absorptivity and fluorescence quantum yield in CHCl$_3$ (ε = 50 800 M^{-1} cm^{-1}, Φ_{F} = 0.008) relative to those of **2** (ε = 115 700 M^{-1} cm^{-1}, Φ_{F} = 1.0). The marked difference in fluorescence quantum yields is consistent in solvents spanning a broad range of polarities from toluene to dimethyl sulfoxide (Table S1 and Fig. S1†), and derives from a decrease in the radiative rate constant for **1** ($k_{\mathrm{F}} = \Phi_{\mathrm{F}}/\tau$, 3.8 × 10^7 s^{-1}, in CHCl$_3$) compared with that of its analog **2** (k_{F} = 1.9 × 10^8 s^{-1}). These results contrast with the observations of Burgess and co-workers on a related 8-trifluoromethylated BODIPY dye bearing chlorine substituents in the 3- and 5-positions, which shows high fluorescence (Φ_{F} > 0.5) and small Stokes shifts (< 30 nm).[19] Taken together, the polarity-independent low quantum yields, comparatively small radiative rate constant and large Stokes shift for **1** may be indicative of significant differences between the geometry of **1** in its S$_0$ and S$_1$ states, leading to an unfavorable Franck–Condon factor.

Most strikingly, although the molecularly dispersed dilute solutions of **1** are non-emissive, increases in concentration leading to the formation of aggregates result in a striking AIEE phenomenon for **1** (Fig. 4, and see ESI†). CF$_3$-BODIPY **1** is virtually non-emissive (Φ_{F} = 0.003) in pure acetonitrile, which is a good solvent for **1**. Progressively increasing the volume fraction of water, a non-solvent, in acetonitrile does not affect its spectrum until the solution consists of 85% water. The emission abruptly increases at higher water fractions (f_{w} > 90%), with the appearance of a new sharp emission band at *ca.* 625 nm (Fig. 4, left). At a f_{w} of 90%, the fluorescence intensity is enhanced over 40-fold (Φ_{F} = 0.06) relative to the pure acetonitrile solution. This increase in fluorescence intensity coincides with the formation of colloidal aggregates (*ca.* 188 nm by DLS, see ESI†), confirming that **1** is AIEE-active. The absorption
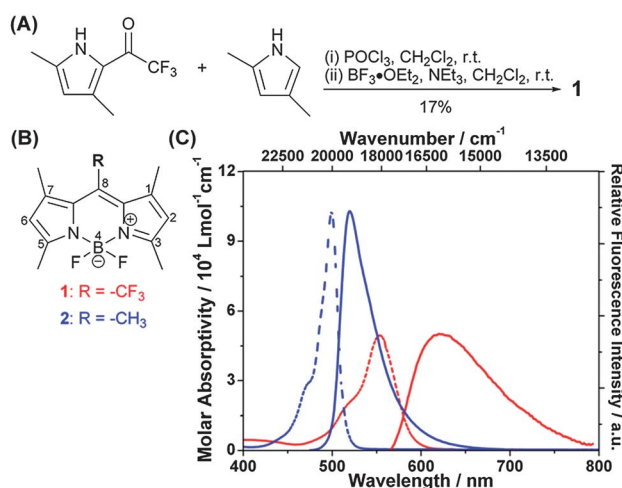
Fig. 2 (A) Synthesis of CF$_3$-BODIPY **1**. (B) Chemical structures of *meso*-substituted BODIPYs **1** and **2**. (C) Absorption (dotted lines) and emission (solid lines) spectra of **1** (red) and **2** (blue) in CHCl$_3$ solutions (2 × 10^{-5} mol L^{-1}). Excitation at 530 nm for **1** and 460 nm for **2**, respectively. The emission spectrum of **1** is magnified 40-fold.
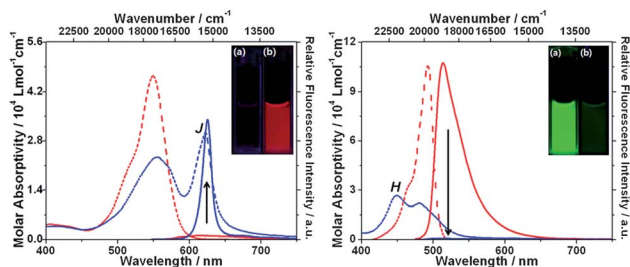
Fig. 4 Absorption (dotted lines) and emission (solid lines) spectra of **1** (left) and **2** (right) at concentrations of 2×10^{-5} mol L^{-1} in CH_3CN (red) and CH_3CN-H_2O solution (blue, $CH_3CN-H_2O = 1:99$ (v/v)). Excitation at 530 nm for **1** and 460 nm for **2**, respectively. Inset shows photographs of each solution (a: CH_3CN, b: $CH_3CN-H_2O = 1:99$ (v/v)) under irradiation at 365 nm.

spectrum of the CH_3CN-H_2O colloidal suspension (1 : 99 v/v, Fig. 4, left) shows its narrow absorption band at 623 nm and an intense aggregate emission band that is merely 2 nm (51 cm^{-1}) to the red of the former, and also remarkably narrow (full width at half-maximum height, fwhm, is 385 cm^{-1}). The fluorescence lifetime τ_F is increased from 0.20 ns in solution to 0.40 ns in the nanoparticle suspension, reflecting a substantial increase in the fluorescence rate constant $k_F = \Phi_F/\tau$ from 1.6×10^7 s^{-1} in solution to 1.5×10^8 s^{-1} as aggregates. Taken together, these photophysical features, denoted as "J" in Fig. 4, left are characteristic of J-aggregates.[9]

By comparison, the absorption and emission behavior of aggregated **2** in CH_3CN–water mixtures is typical of dyes of the BODIPY family. The emission intensity of **2**, which is strongly fluorescent in dilute solutions, decreased markedly upon increasing f_w in CH_3CN–water mixtures (Fig. 4, right). This decrease is accompanied by a substantial reduction in k_F of the aggregates (3.2×10^7 s^{-1}) compared with the solution value (1.5×10^8 s^{-1}). Finally, and contrary to what was found for **1**, the absorption spectra of **2** in CH_3CN-H_2O ($f_w > 90\%$) show the appearance of a new absorption band ($\lambda_{max} = 451$ nm) to the blue of the monomer band ($\lambda_{max} = 492$ nm), denoted as "H" in Fig. 4, right.

The X-ray crystal structures reveal the differences in the packing arrangements between the two dyes (Fig. 5 and 6). Both solid-state organizations are characterized by slipped stacks of boraindacene planes with significant π–π interactions. Possibly due to the greater bulk of the trifluoromethyl group,[20] the distance between these parallel aromatic planes is slightly greater for **1** (3.70 Å) than for **2** (3.55 Å). However, bulk alone cannot rationalize the remarkable solid-state luminescence of **1**, given that analogues of **1** substituted at the 8-position by phenyl, naphthyl or pyrenyl groups in place of trifluoromethyl are highly luminescent in solution but suffer from quenching in condensed states.[8a,21] In columnar stacks of **1**, the ground state dipole moments, which align with the $B \rightarrow C_{meso}$ vectors, are parallel, whereas **2** packs in antiparallel stacks. Two factors may contribute to favor parallel stacking for **1** instead of antiparallel stacking as for **2**. First, the presence of an electron-acceptor group at the *meso*-position lowers the magnitude of the ground state dipole moment from 4.63 D for **2** to 1.97 D for **1**,[16] reducing the electrostatic cost for the parallel stacking of **1**. Secondly, fluorophilic and/or fluorophobic interactions evident within the crystal structure can likely favor the proximity between the trifluoromethyl groups on adjacent dyes that the parallel stacking enforces.

Nevertheless, the key difference between the solid-state structures of **1** and **2** is the orientation of the transition dipoles relative to the stacking axes. The $S_0 \leftrightarrow S_1$ transition dipole of BODIPY dyes is parallel with its long molecular axis that spans the 2- and 6-positions, and perpendicular to the C_2 axis of symmetry.[11] While both dyes **1** and **2** adopt coplanar inclined arrangements of their transition dipoles, a slip angle of 36° is observed for the former (Fig 5C), whereas a slip angle of 65° is found for the latter (Fig. 6C). These arrangements and the spectroscopic features of aggregates are in perfect agreement with Kasha's molecular exciton model, and correspond to textbook cases of J-type ($\theta < 54.7°$) and H-type ($\theta > 54.7°$) packings for **1** and **2**, respectively.[10]

To illustrate the potential of AIEE arising from **1** in solid-state applications, we examined the photophysical properties of
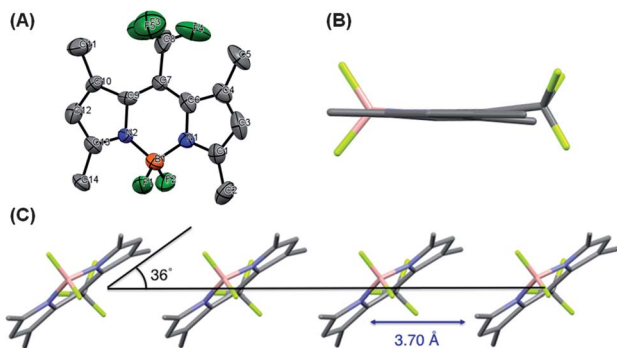

Fig. 5 Top (A) and side (B) views of the molecular structure of **1**, with the thermal ellipsoids set at 50% probability. (C) Packing diagram of **1**. H atoms are omitted for clarity.
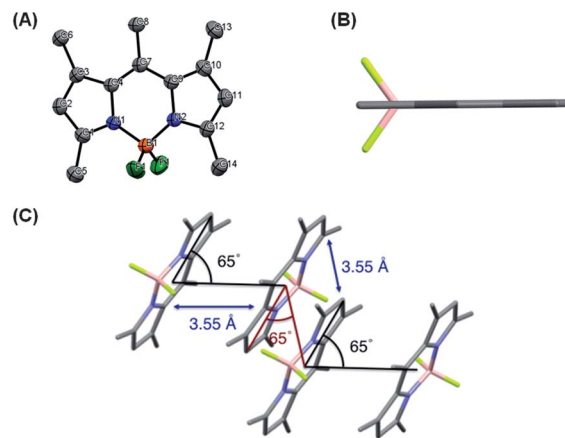

Fig. 6 Top (A) and side (B) views of the molecular structure of **2**, with the thermal ellipsoids set at 50% probability. (C) Packing diagram of **2**. H atoms are omitted for clarity.

dye **1** in solid solutions, and compared them to those of its non-fluorinated congener **2**. Thin solid films of poly(methyl methacrylate) (PMMA) doped with varying concentrations of the dyes were prepared.

For dye **1**, as in the case of suspended molecular aggregates in CH_3CN–H_2O mixtures, the emission bands show a marked concentration dependence, with the intensity of the red-shifted band continuously increasing as a function of its concentration in PMMA (Fig. 7A, and see ESI†). By contrast, the fluorescence intensities of thin PMMA films doped with **2** saturate at a concentration of *ca.* 5 wt% before rapidly decreasing at higher concentration, also reflecting the behavior observed for molecular aggregates of **2** in CH_3CN–H_2O mixtures. An additional advantage associated with the introduction of per-fluorinated functional groups in **1** is its increased photostability since electron-withdrawing substituents raise ionization potentials, as previously demonstrated.[22] Thin solid films of PMMA doped with either **1** or **2** were irradiated with a 150 W steady-state Xe lamp. Films of **1** retained over 99% of their original fluorescence intensity after 2 h of continuous irradiation (Fig. 7B), but under the same conditions films of **2** suffered from more than 30% degradation. The combination of high luminescence in aggregated condensed phases and remarkable photostability are required for applications including solid-state dye lasers and solar energy capture, for which dyes that follow BODIPY **1**'s design could offer significant potential.

Conclusions

In summary, the *meso*-CF$_3$-substituted BODIPY **1** shows enviable aggregation-induced emission enhancement (AIEE) due to the formation of J-aggregates that result in narrow, red-shifted transitions and increased quantum efficiency. For the first time among dyes of the BODIPY family, the molecular packing responsible for the formation of these aggregates was definitively established by an X-ray diffraction study. CF$_3$-BODIPY **1** presents one of the clearest examples to date of a solid-state structure in which the transition dipoles of neighboring dyes adopt a coplanar inclined arrangement, with a slip angle

inferior to 54.7°, that is characteristic of a J-type packing consistent with excitonic coupling theory.[10] These features, and the design principles embedded in CF$_3$-BODIPY **1** constitute a valuable addition to the toolbox for the development of solid-state devices based on luminescent J-aggregates.

Acknowledgements

Notes and references

1 (*a*) R. P. Haughland, *Handbook of Fluorescent Probes and Research Products*, Molecular Probes, Inc., Eugene, OR, 9th edn, 2002; (*b*) M. S. T. Gonçalves, *Chem. Rev.*, 2009, **109**, 190.

2 (*a*) A. Costela, I. García-Moreno, C. Gomez, R. Sastre, F. Amat-Guerri, M. Liras, F. L. Arbeloa, J. B. Prieto and I. L. Arbeloa, *J. Phys. Chem. A*, 2002, **106**, 7736; (*b*) D. Zhang, V. Martín, I. García-Moreno, A. Costela, M. E. Pérez-Ojeda and Y. Xiao, *Phys. Chem. Chem. Phys.*, 2011, **13**, 13026.

3 (*a*) N. Boens, V. Leen and W. Dehaen, *Chem. Soc. Rev.*, 2012, **41**, 1130; (*b*) A. C. Benniston and G. Copley, *Phys. Chem. Chem. Phys.*, 2009, **11**, 4124.

4 (*a*) G. Ulrich, R. Ziessel and A. Harriman, *Angew. Chem., Int. Ed.*, 2008, **47**, 1184; (*b*) A. Loudet and K. Burgess, *Chem. Rev.*, 2007, **107**, 4891.

5 (*a*) D. Tleugabulova, Z. Zhang and J. D. Brennan, *J. Phys. Chem. B*, 2002, **106**, 13133; (*b*) Y. Tokoro, A. Nagai and Y. Chujo, *Tetrahedron Lett.*, 2010, **51**, 3451.

6 T. Ozdemir, S. Atilgan, I. Kutuk, L. T. Yildirim, A. Tulek, M. Bayindir and E. U. Akkaya, *Org. Lett.*, 2009, **11**, 2105.

7 S. Frein, F. Camerel, R. Ziessel, J. Barberá and R. Deschenaux, *Chem. Mater.*, 2009, **21**, 3950.

8 (*a*) R. Hu, E. Lager, A. Aguilar-Aguilar, J. Liu, J. W. Y. Lam, H. H. Y. Sung, I. D. Williams, Y. Zhong, K. S. Wong, E. Peña-Cabrera and B. Z. Tang, *J. Phys. Chem. C*, 2009, **113**, 15845; (*b*) J. Gierschner and S. Y. Park, *J. Mater. Chem. C*, 2013, **1**, 5818; (*c*) D. Ding, K. Li, B. Liu and B. Z. Tang, *Acc. Chem. Res.*, 2013, **46**, 2441.

9 (*a*) F. Würthner, T. E. Kaiser and C. R. Saha-Möller, *Angew. Chem., Int. Ed.*, 2011, **50**, 3376; (*b*) E. E. Jelley, *Nature*, 1936, **138**, 1009; (*c*) G. Scheibe, *Angew. Chem.*, 1936, **49**, 563.

10 (*a*) M. Kasha, H. R. Rawls and M. A. El-Bayoumi, *Pure Appl. Chem.*, 1965, **11**, 371; (*b*) A. S. Davydov, *Theory of Molecular Excitons*, Plenum Press, New York, 1971.

11 (*a*) F. Bergström, I. Mikhalyov, P. Hägglöf, R. Wortmann, T. Ny and L. B.-Å. Johansson, *J. Am. Chem. Soc.*, 2002, **124**, 196; (*b*) I. Mikhalyov, N. Gretskaya, F. Bergström and L. B.-Å. Johansson, *Phys. Chem. Chem. Phys.*, 2002, **4**, 5663; (*c*) D. Marushchak, S. Kalinin, I. Mikhalyov, N. Gretskaya and L. B.-Å. Johansson, *Spectrochim. Acta, Part A*, 2006, **65**, 113.

12 T. T. Vu, M. Dvorko, E. Y. Schmidt, J.-F. Audibert, P. Retailleau, B. A. Trofimov, R. B. Pansu, G. Clavier and R. Méallet-Renault, *J. Phys. Chem. C*, 2013, **117**, 5373.
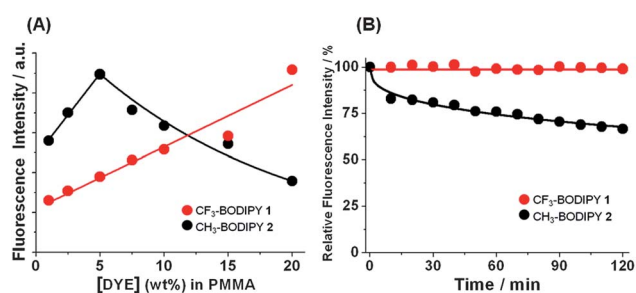

Fig. 7 (A) Relationship between fluorescence intensity at maximum wavelength and various concentrations of **1** and **2** (from 1 to 20 wt%) dopants in PMMA films. Excitation at 530 nm and 460 nm for **1** and **2**, respectively. (B) Photostability tests showing the relative fluorescence intensity of thin films with **1** and **2** as a function of photoirradiation time. Spin-coated thin films having similar optical density (0.02 ± 0.002) were irradiated at 460 nm.

13 T. T. Vu, S. Badré, C. Dumas-Verdes, J.-J. Vachon, C. Julien, P. Audebert, E. Y. Senotrusova, E. Y. Schmidt, B. A. Trofimov, R. B. Pansu, G. Clavier and R. Méallet-Renault, *J. Phys. Chem. C*, 2009, **113**, 11844.

14 (*a*) J.-H. Olivier, J. Widmaier and R. Ziessel, *Chem.–Eur. J.*, 2011, **17**, 11709; (*b*) H. Lu, Z. Xue, J. Mack, Z. Shen, X. You and N. Kobayashi, *Chem. Commun.*, 2010, **46**, 3565; (*c*) F. Camerel, L. Bonardi, M. Schmutz and R. Ziessel, *J. Am. Chem. Soc.*, 2006, **128**, 4548.

15 B. Guo, X. Peng, A. Cui, Y. Wu, M. Tian, L. Zhang, X. Chen and Y. Gao, *Dyes Pigm.*, 2007, **73**, 206.

16 Gas-phase values calculated after geometric optimization at the B3LYP 6-311++ G(d,p) level of theory. See the ESI† for details.

17 (*a*) K. Rurack, M. Kollmannsberger and J. Daub, *Angew. Chem., Int. Ed.*, 2001, **40**, 385; (*b*) S. Atilgan, Z. Ekmekci, A. L. Dogan, D. Guc and E. U. Akkaya, *Chem. Commun.*, 2006, 4398.

18 (*a*) M. Wada, S. Ito, H. Uno, T. Murashima, N. Ono, T. Urano and Y. Urano, *Tetrahedron Lett.*, 2001, **42**, 6711; (*b*) Z. Shen, H. Rohr, K. Rurack, H. Uno, M. Spieles, B. Schulz, G. Reck and N. Ono, *Chem.–Eur. J.*, 2004, **10**, 4853; (*c*) S. Goeb and R. Ziessel, *Org. Lett.*, 2007, **9**, 737.

19 (*a*) L. Li, B. Nguyen and K. Burgess, *Bioorg. Med. Chem. Lett.*, 2008, **18**, 3112; (*b*) L. N. Sobenina, A. M. Vasil'tsov, O. V. Petrova, K. B. Petrushenko, I. A. Ushakov, G. Clavier, R. Meallet-Renault, A. I. Mikhaleva and B. A. Trofimov, *Org. Lett.*, 2011, **13**, 2524.

20 According to the Taft scale, the CF$_3$ group ($E_S = -2.40$) is larger than the CH$_3$ group ($E_S = -1.24$); I. Ojima, *Fluorine in Medicinal Chemistry and Chemical Biology*, Wiley, New York, 2009.

21 (*a*) R. Ziessel, C. Goze, G. Ulrich, M. Césario, P. Retailleau, A. Harriman and J. P. Rostron, *Chem.–Eur. J.*, 2005, **11**, 7366; (*b*) J. Bañuelos, I. J. Arroyo-Córdoba, I. Valois-Escamilla, A. Alvarez-Hernández, E. Peña-Cabrera, R. Hu, B. Z. Tang, I. Esnal, V. Martínez and I. López Arbeloa, *RSC Adv.*, 2011, **1**, 677.

22 (*a*) K. Umezawa, Y. Nakamura, H. Makino, D. Citterio and K. Suzuki, *J. Am. Chem. Soc.*, 2008, **130**, 1550; (*b*) Y. Kim and T. M. Swager, *Chem. Commun.*, 2005, 372; (*c*) G. Y. Mitronova, V. N. Belov, M. L. Bossi, C. A. Wurm, L. Meyer, R. Medda, G. Moneron, S. Bretschneider, C. Eggeling, S. Jakobs and S. W. Hell, *Chem.–Eur. J.*, 2010, **16**, 4477; (*d*) Y. Kim, J. E. Whitten and T. M. Swager, *J. Am. Chem. Soc.*, 2005, **127**, 12130.